

Optical Engineering

OpticalEngineering.SPIEDigitalLibrary.org

Ultrasmall in-plane demultiplexer enabled by an arrayed one-dimensional photonic crystal nanobeam cavity

Daquan Yang
Xin Chen
Xuan Zhang

SPIE.

Daquan Yang, Xin Chen, Xuan Zhang, "Ultrasmall in-plane demultiplexer enabled by an arrayed one-dimensional photonic crystal nanobeam cavity," *Opt. Eng.* **57**(10), 107103 (2018), doi: 10.1117/1.OE.57.10.107103.

Ultrasmall in-plane demultiplexer enabled by an arrayed one-dimensional photonic crystal nanobeam cavity

Daquan Yang,^{a,b,*} Xin Chen,^a and Xuan Zhang^a

^aBeijing University of Posts and Telecommunications, School of Information and Communication Engineering, Beijing, China

^bBeijing University of Posts and Telecommunications, State Key Laboratory of Information Photonics and Optical Communications, Beijing, China

Abstract. We propose a design for silicon-on-chip integrated eight-channel wavelength division multiplexing (WDM) demultiplexer, which consists of parallel-arrayed one-dimensional (1-D) photonic crystal nanobeam cavities (PCNCs) with high- Q over 10^5 and large free spectral range of ~ 200 nm. To the best of our knowledge, this is for the first time that a 1-D PCNC-based demultiplexer is presented. The performance of the device is investigated theoretically by using three-dimensional finite-difference time-domain method. To enable eight-channel parallel arrayed 1-D PCNCs to be coupled to on-chip optical networks for higher integration and multiplex application, an 1×8 taper-type equal optical power splitter is used to connect all channels simultaneously. The total device footprint is as small as $12 \mu\text{m} \times 15 \mu\text{m}$ (width \times length), which is decreased by five times compared to that per channel in the recent two-dimensional (2-D) PC-based demultiplexer. Moreover, the average channel spacing smaller than 115 GHz is achieved, which is more than two times smaller than that of 2-D PC nanocavity devices, demonstrating that the arrayed nanocavities have the potential for developing ultracompact 100-GHz spaced filters in a dense WDM system. Thus, we believe that the results demonstrated in this work is promising for the future on-chip photonics integrated circuits and optical communication systems. © The Authors. Published by SPIE under a Creative Commons Attribution 3.0 Unported License. Distribution or reproduction of this work in whole or in part requires full attribution of the original publication, including its DOI. [DOI: [10.1117/1.OE.57.10.107103](https://doi.org/10.1117/1.OE.57.10.107103)]

Keywords: one-dimensional photonic crystals nanobeam cavities; wavelength division multiplexing demultiplexer; optical interconnects; silicon nanophotonics.

Paper 181059 received Jul. 23, 2018; accepted for publication Sep. 26, 2018; published online Oct. 20, 2018.

1 Introduction

Over the past decades, with the increasing demand for bandwidth, it has become a significant trend to develop optics communication systems for large-capacity and high-efficiency data transmission. Wavelength division multiplexing (WDM) technology plays a very important role in longhaul optics communication systems because it supports large-capacity data transmission with high reliability.^{1–6} So far, a variety of optical WDM demultiplexers used in silicon (Si) photonics have been proposed and demonstrated, such as Si microring demultiplexers,⁷ Si arrayed waveguide grating (AWG) demultiplexers,^{8–10} Si multimode interference (MMI) demultiplexers,^{11,12} and Si Mach–Zehnder switches demultiplexers.^{13–15} However, the footprint of these WDM demultiplexers is too large, and therefore difficult to integrate with other nanoscale optical components. Thus, recently attention has turned to developing on-chip compact WDM demultiplexers with an ultrasmall footprint.¹⁶

Silicon photonic crystals (PC), artificial periodic structures with high refractive index contrast in dielectric media, and a periodicity in the wavelength scale of light have attracted great interest because of their potential to control light propagation effectively in a short distance, which can lead to very compact devices. Consequently, silicon PC is a promising candidate for achieving ultracompact WDM demultiplexers. To realize smaller WDM demultiplexers, those based on Si PC are being developed.^{17–24} For example, Song et al.¹⁸ demonstrated two-dimensional (2-D) PC cavities-based 16-channel WDM demultiplexer with 628-GHz channel spacing, and the

footprint of per channel is $12 \mu\text{m}^2$. Takahashi et al.²¹ demonstrated 2-D PC cavities-based 32-channel out-of-plane WDM demultiplexer with 100-GHz channel spacing, and the footprint of per channel is $\sim 130 \mu\text{m}^2$. Ooka et al.²⁴ demonstrated 2-D PC cavities-based eight-channel in-plane WDM demultiplexer with 267-GHz channel spacing, and the footprint of per channel is $110 \mu\text{m}^2$. Among these Si PC-based WDM demultiplexers mentioned above, all of them are based on 2-D PC cavity platforms.

Compared with 2-D PC cavities, one-dimensional (1-D) PC nanobeam cavities (PCNCs) have been recently demonstrated as a competitive platform for large-scale on-chip photonic integration, owing to their attractive properties of ultracompact footprint, ultrahigh Q/V (Q and V are cavity quality factor and mode volume, respectively), and high integrability with optical bus-waveguides and circuits.^{25–36} Thus, to achieve an ultracompact WDM demultiplexer with much smaller footprint, a method for the dense integration of ultracompact 1-D PCNCs-based WDM demultiplexer is proposed on a monolithic silicon chip. The proposed demultiplexer device consists of multiple channels of parallel-arrayed 1-D PCNCs units. The adjacent channels are separated with small air-gap separations. Each channel consists of a high- Q 1-D PCNC with different cavity length to extract transmitted light with a specific resonant wavelength. To enable all parallel-arrayed 1-D PCNCs units to be interrogated simultaneously, a $1 \times N$ equal power splitter is used in the input port of the device. The performance of the device is investigated theoretically by using three-dimensional finite-difference time-domain (3-D FDTD) simulation (a commercial software package, Lumerical FDTD Solutions). The results show that the presented eight-channel WDM

*Address all correspondence to: Daquan Yang, E-mail: yangdq5896@163.com

demultiplexer with dense channel spacing smaller than 115 GHz is achieved. Moreover, the footprints per channel are $22.5 \mu\text{m}^2$, which is decreased by more than five times compared to the per channel in the recent 2-D PC-based WDM demultiplexers.^{21,24} In addition, it is worth mentioning that, by changing the cavity length on the subnanometer scale, the peak wavelengths at 100-GHz spacing in the wavelength range between 1330 and 1420 nm can be successfully designed, which is potentially a promising platform for developing ultracompact 100-GHz spaced dense WDM system with more than 100 channels.

The paper is organized as follows. Section 2 describes the design of the proposed eight-channel WDM demultiplexers based on parallel-arrayed 1-D PCNCs units. Section 3 shows the performance discussion and analysis of the proposed WDM demultiplexers based on the results obtained by using 3-D FDTD. Section 4 draws a brief conclusion of the paper.

2 Design

Figure 1(a) shows the proposed eight-channel WDM demultiplexer in the upper 220-nm-thick silicon layer of a silicon-on-insulator (SOI) substrate. The refractive index of the silicon layer and silica substrate is $n_{\text{Si}} = 3.46$ and $n_{\text{SiO}_2} = 1.45$, respectively. A 1×8 optical power splitter (OPS) divides the input signal power into eight channels, respectively. The width of OPS (w_{in}) is $12 \mu\text{m}$ and the length of tapered waveguide (l_{taper}) is $10 \mu\text{m}$. And the input port width of the eight tapered silicon waveguides are 4.60, 1.15, 0.89, 0.86, 0.86, 0.89, 1.15, and $4.60 \mu\text{m}$ from top to bottom. By using 3-D FDTD method, Fig. 2 shows the composed transmission spectra of each output port in the proposed 1×8 OPS. It is worth mentioning that the insertion loss includes the coupling losses, the excess losses, and the propagation losses.^{37,38} All the insertion losses for each output port of the proposed 1×8 OPS at wavelength of $\sim 1550 \text{ nm}$ are

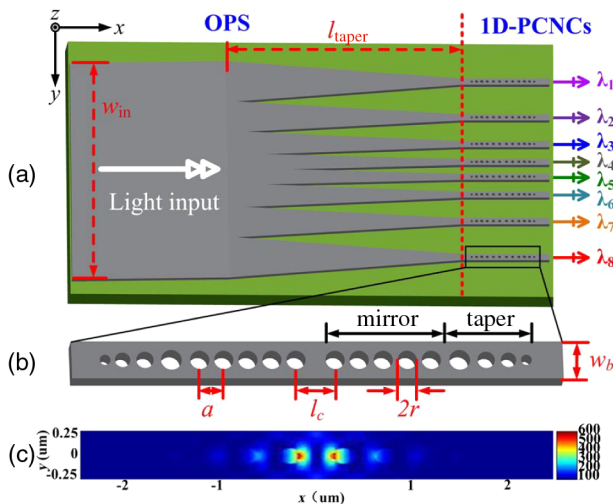


Fig. 1 (a) Schematic illustration of an eight-channel WDM demultiplexer based on parallel-arrayed 1-D PCNC units. For each channel, only a single 1-D PCNC unit with different cavity length is consisted. In the input port, a 1×8 taper-type OPS is used to connect all channels simultaneously. The footprint of the whole eight-channel WDM demultiplexer, including the OPS, is as small as $\sim 12 \mu\text{m} \times 15 \mu\text{m}$ (width by length). (b) Zoom-in illustration of a single 1-D PCNC unit. (c) Electric field distribution of single channel at resonant wavelength.

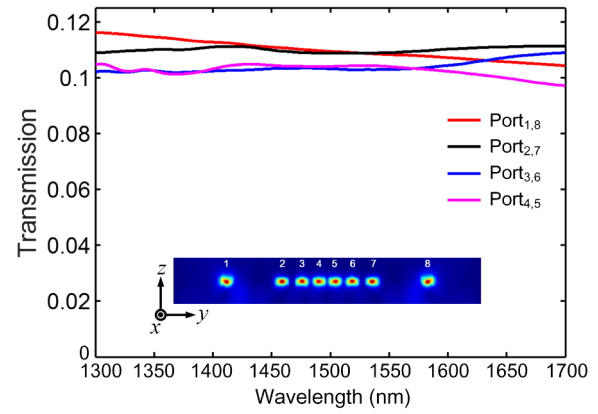


Fig. 2 3-D FDTD simulation composed transmission spectra of each channel in the proposed 1×8 OPS. The inset is the cross-section of electric field profile for the fundamental TE-like mode propagating through the output ports of the splitter in $y - z$ plane.

9.61, 9.64, 9.86, 9.83, 9.83, 9.86, 9.64, and 9.61 dB, respectively, which are the best values obtained from the optimized simulation. The excess loss is 0.69 dB. We have also captured the output profiles of the 1×8 OPS. The inset in Fig. 2 is the cross-section of electric field profile for the fundamental TE-like mode propagating through the output ports of the splitter in $y - z$ plane. It can be seen that the field intensity of each output is nearly uniform. And the calculated output uniformity of the splitter at a wavelength of $\sim 1550 \text{ nm}$ is better than 0.25 dB.

The 1-D PCNC arrays consists of eight parallel-arrayed 1-D PCNC units separated by air-gap. A single 1-D PCNC unit is shown in Fig. 1(b), which consists of a single row of air ($n_{\text{air}} = 1.0$) hole gratings embedded in a nanobeam silicon waveguide. For all of the eight 1-D PCNC units, the width and thickness of the silicon nanobeam waveguide are the same as $w_b = 500 \text{ nm}$ and $h = 220 \text{ nm}$, respectively. Next, we introduce a defect region into the cavity by gradually increasing the periodicity (hole-to-hole distance) and hole diameter for each segment starting from a pair of outer holes and symmetrically moving toward the center. When the feature size of a segment is enlarged, the band-gap is redshifted, resulting in a graded photonic band, as shown in Fig. 3. This allows confining a resonant mode (ω_{res}) in the defect region: the resonant mode is coupled to the evanescent Bloch modes within the photonic band-gaps (PBG) in the cavity center, effectively trapping it between a pair of Bragg mirrors. Here, the number of the air-hole gratings (N_m) in the mirror region and the number of the air-hole gratings (N_t) in the tapered region of each unit are the same as $N_m = 5$ and $N_t = 4$, respectively. And the air-hole gratings radii (r) and the periodicity (a) in the mirror region are the same as $r = 85 \text{ nm}$ and $a = 350 \text{ nm}$, respectively. All the air-hole gratings radii in the tapered region that are the same linearly decreased from inside to outside as 95, 80, 65, and 50 nm , respectively; all the periodicities in the tapered region that are the same linearly decreased from inside to outside as 310, 290, 270, and 250 nm , respectively. The only difference among these eight parallel-arrayed 1-D PCNC units is that each unit has a different cavity length (l_{c1} , l_{c2} , l_{c3} , l_{c4} , l_{c5} , l_{c6} , l_{c7} , and l_{c8} referring to the cavity length of cavity unit 1, 2, 3, 4, 5, 6, 7, and 8, respectively, being 1 the unit at the top channel and 8 the unit at the bottom

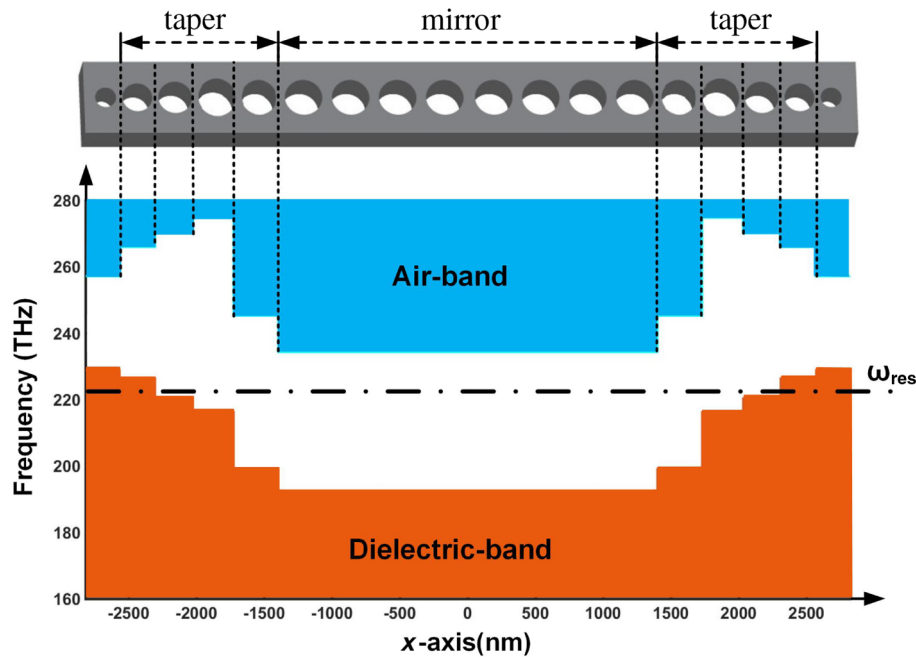


Fig. 3 Diagram of tapered PBG for a typical 1-D PCNC unit with cavity length $l_c = 350$ nm.

channel) to extract transmitted light with a different wavelength ($\lambda_1, \lambda_2, \lambda_3, \lambda_4, \lambda_5, \lambda_6, \lambda_7,$ and λ_8). Here, the cavity length (l_c) is defined as the distance between the two adjacent air holes in the cavity center [Fig. 1(b)]. As seen in Fig. 1(c), the optical field is well-localized in the dielectric zone between the two center holes.

The Q -factors optimization of a single 1-D PCNC unit by using 3-D FDTD is shown in Fig. 4. The number of the air-hole gratings in the mirror section and the number of the air-hole gratings in the tapered section are investigated in detail. The optimized Q -factor of a 1-D PCNC unit over 10^5 can be achieved. The Q value is higher than that obtained with an L_n nanocavity ($\sim 10^3$)²¹ and width-modulated nanocavity ($\sim 10^4$)²⁴ in 2-D PC slabs. In this work, in order to save the simulation time of the transmission calculation, we used a high transmission but low Q geometry: the number of gratings was chosen to be $N_m = 5$, and $N_t = 4$ in the mirror region and taper region, respectively. Figure 5 summarizes the calculated cavity resonant wavelength and free spectral range (FSR) as a function of the cavity length changed from $l_c = 300$ nm to $l_c = 500$ nm. As expected, with the cavity length increased, the cavity resonant wavelength moves toward longer wavelength, due to the increase in high-dielectric material in the cavity center region.³⁹ As seen, with proper engineering of the cavity length of 1-D PCNC unit, an arbitrary resonant wavelength ranging from 1240 to 1430 nm can be obtained, indicating that WDM demultiplexer can be operated with flexible design. In addition, the cavity FSR increases with the increasing cavity length. When the cavity length $l_c = 500$ nm, the cavity FSR as large as 197 nm can be achieved, which is significantly increased compared to previous design,⁴⁰ indicating that a wide enough bandwidth is provided to design a WDM demultiplexer with as many channels as possible. This indicates that a dense WDM demultiplexer can be achieved. Here, it is worth mentioning that the footprint

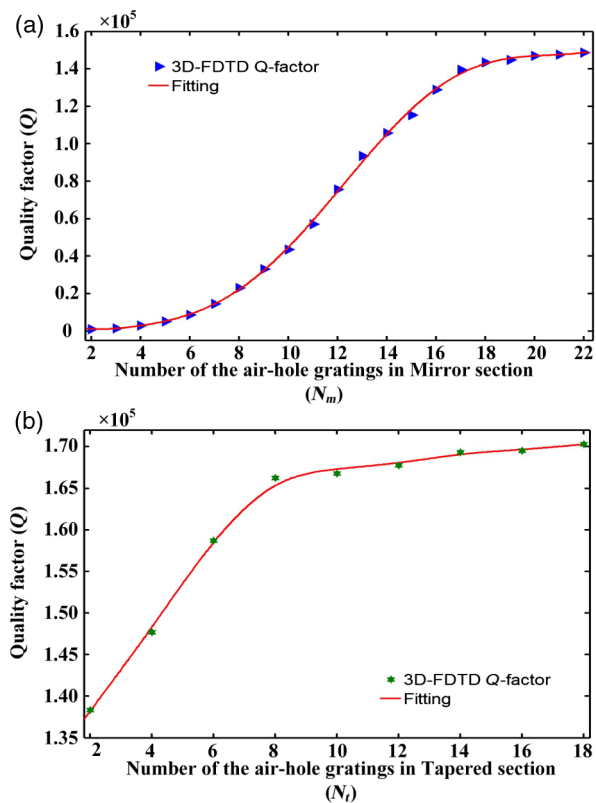


Fig. 4 3-D FDTD calculated Q -factors as a function of (a) the number of the air-hole gratings (N_m) in the mirror section changed from $N_m = 2$ to $N_m = 22$, while the number of the air-hole gratings (N_t) in the tapered section is kept fixed as $N_t = 3$; and (b) the number of the air-hole gratings (N_t) in the tapered section changed from $N_t = 2$ to $N_t = 10$, while the number of the air-hole gratings (N_m) in the mirror section is kept fixed as $N_m = 21$.

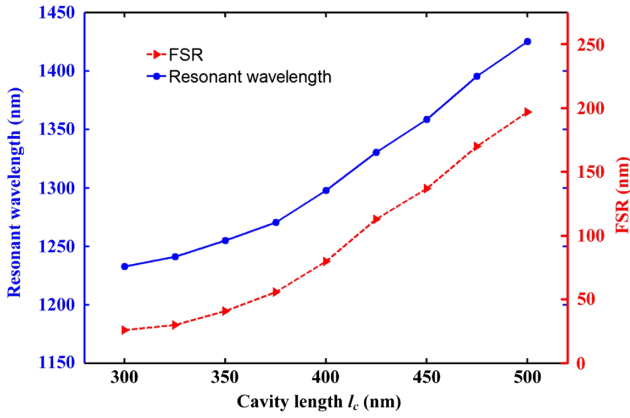


Fig. 5 Cavity resonant wavelength and FSR as a function of the cavity length (l_c) changed from 300 to 500 nm, where $N_m = 5$, $N_t = 4$. The air-hole gratings radii and periodicities in the mirror region and the tapered region are kept fixed.

of a single 1-D PCNC unit is ultracompact as small as $\sim 3 \mu\text{m}^2$ [with $l_c = 500$ nm, $N_m = 5$, and $N_t = 4$ shown in Fig. 1(b)], which is decreased more than one order of magnitude compared with previous designs based on 2-D PC nanocavities ($\sim 100 \mu\text{m}^2$).^{21,24} Thus, the proposed parallel-arrayed 1-D PCNC units with high Q , large FSR, and ultrasmall footprint is potentially a promising platform for high-density integrated dense WDM design and on-chip integrated WDM optical communication systems.

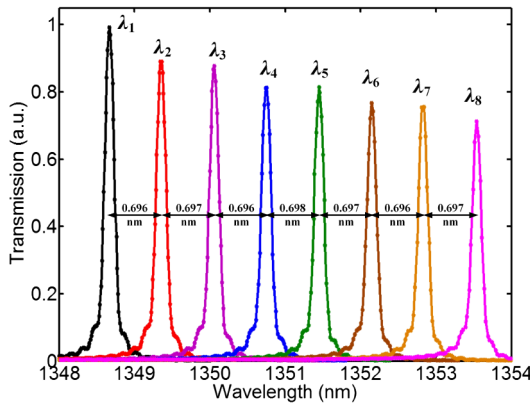


Fig. 6 3-D FDTD normalized transmission spectra of a typical eight-channel WDM demultiplexer device with uniform channel spacing smaller than 115 GHz ($\lambda < 0.7$ nm).

3 Discussion

3-D FDTD simulations are performed to numerically study the performances of the proposed eight-channel WDM demultiplexer based on parallel-arrayed 1-D PCNC units. There is a linear relationship between the cavity length and the output wavelength (λ). In this work, in order to obtain uniform channel spacing, the cavity length of each cavity unit in the channel from top to bottom is $l_{c1} = 409.0$ nm, $l_{c2} = 409.8$ nm, $l_{c3} = 410.6$ nm, $l_{c4} = 411.4$ nm, $l_{c5} = 412.2$ nm, $l_{c6} = 413.0$ nm, $l_{c7} = 413.8$ nm, and $l_{c8} = 414.6$ nm, respectively. Figure 6 shows the composed transmission spectra of the proposed eight-channel WDM demultiplexer. As expected, the proposed device can divide the input light wavelength into eight different wavelengths with $\lambda_1 = 1348.67$ nm, $\lambda_2 = 1349.36$ nm, $\lambda_3 = 1350.06$ nm, $\lambda_4 = 1350.75$ nm, $\lambda_5 = 1351.45$ nm, $\lambda_6 = 1352.14$ nm, $\lambda_7 = 1352.84$ nm, and $\lambda_8 = 1353.54$ nm, where the uniform channel spacing is smaller than 115 GHz (< 0.7 nm). The insertion losses of each output port of the proposed eight-channel demultiplexer at the corresponding resonant wavelength of $\lambda_1, \lambda_2, \lambda_3, \lambda_4, \lambda_5, \lambda_6, \lambda_7$, and λ_8 are 14.12, 14.28, 14.30, 14.33, 13.93, 13.19, 13.71, and 13.57 dB, respectively. The excess loss, namely the total loss, is 4.88 dB. The power division ratio, defined as the ratio of the minimum and maximum power of all output powers, is 1.14 dB. The channel isolation levels, defined as the level difference of the output power in all channels at the same resonant wavelength, are better than 10 dB for all the different resonant wavelengths of the proposed demultiplexer.

In addition, we compare the performance of our device with that of previously reported devices, as shown in Table 1. As seen, we find that the performance of the proposed WDM device based on parallel arrayed 1-D PCNC units are greatly improved compared with other silicon-based WDM devices. The average channel spacing and per-channel footprint are decreased by two times and five times, respectively, compared with that of the recent 2-D PC cavity-based WDM demultiplexer.²⁴ In addition to the small footprint, the structural simplicity of the proposed demultiplexer in this paper lends itself to easier fabrication. The experimental realization of the proposed demultiplexer is generally technically achievable with modern nanofabrication technique, such as electron beam lithography (EBL) technique. Thus, the proposed demultiplexer structure can be experimentally achieved on an SOI platform using the EBL technique, as demonstrated in our previous work.³⁴

Moreover, it is worth mentioning that by changing the cavity length on the subnanometer scale, the peak

Table 1 Performance of various silicon-based WDM schemes.

Structure and platform	Nanocavity	Configuration	Number of channels	Average channel spacing	Footprint of per channel	Ref.
AWG SOI	–	In-plane	8	250 GHz	$1.7 \times 10^4 \mu\text{m}^2$	10
2-D PC SOI	L_3 cavity	Out-of-plane	32	100 GHz	$\sim 130 \mu\text{m}^2$	21
2-D PC SOI	Width modulation cavity	In-plane	8	267 GHz	$110 \mu\text{m}^2$	24
2-D PC SOI	Nanobeam cavity	In-plane	8	115 GHz	$22.5 \mu\text{m}^2$	Present work

Note: SOI, silicon on insulator.

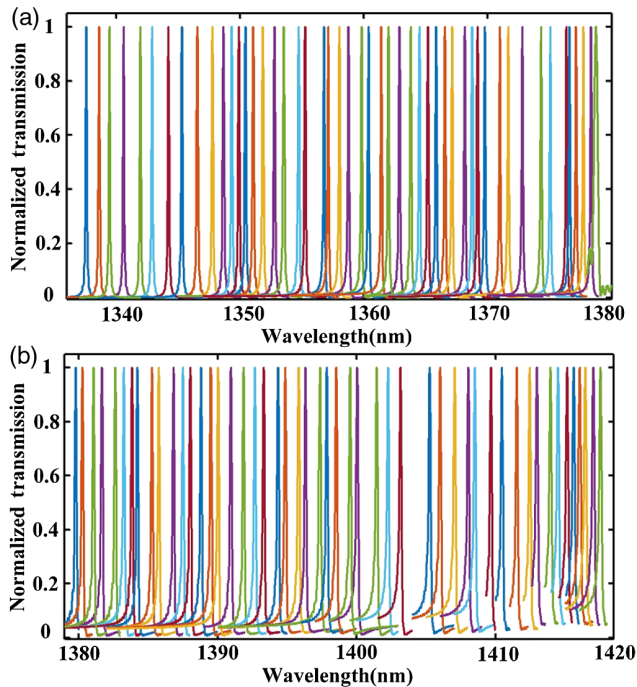


Fig. 7 3-D FDTD composed transmission spectra of a hundred 1-D PCNC units with different cavity length. Here, the transmission spectrum of each cavity unit is normalized independently. The average channel spacing of ~ 100 GHz can be observed in the wavelength ranging from (a) 1330 nm to 1380 nm and (b) 1380 nm to 1420 nm.

wavelengths at 100-GHz spacing in the wavelength range between 1330 and 1420 nm can be successfully controlled, as shown in Fig. 7, which is potentially a promising platform for developing ultracompact 100-GHz spaced dense WDM system with more than 100 channels. However, the insertion loss in the proposed demultiplexer will increase as the channel number increasing. To solve this problem, the feasible methods to minimize the insertion loss are as follows: (1) increasing the transmission efficiency of each channel by further optimizing the structure parameters of the 1-D PCNCs; (2) choosing other optical power splitters with extremely low insertion losses (e.g., MMI-based beam splitter^{12,41}) for the proposed 1-D PC-based demultiplexer to decrease the insertion loss.

4 Conclusion

We have proposed and numerically demonstrated an ultracompact in-plane eight-channel WDM demultiplexer with dense channel spacing smaller than 115 GHz and ultrasmall footprint of $22.5 \mu\text{m}^2$ per channel, using parallel-arrayed 1-D PCNC units. Compared with the 2-D PC nanocavity-based WDM devices, both the average channel spacing and footprint of per channel are significantly decreased. This is achieved thanks to the high- Q and ultracompact size of the 1-D PCNC. In addition, it is important to point out that the method for building an ultracompact WDM device demonstrated in this work is straightforward. And the device structure is very simple. Thus, we believe that the results presented here may widen the highly parallel performance and multiplexed capability of 1-D PCNCs. Moreover, it also may widen the dense integration performance of on-chip integrated photonic devices or integrated optical circuits based on 1-D PCNCs.

Acknowledgments

The authors gratefully acknowledge the support from the National Natural Science Foundation of China (NSFC) (61501053); the Fundamental Research Funds for the Central Universities (2018XKJC05); and the Fund of the State Key Laboratory of Information Photonics and Optical Communications (IPOC2017ZT05), Beijing University of Posts and Telecommunications, China.

References

1. S. Fan et al., "Channel drop tunneling through localized states," *Phys. Rev. Lett.* **80**(5), 960–963 (1998).
2. S. Noda, A. Chutinan, and M. Imada, "Trapping and emission of photons by a single defect in a photonic bandgap structure," *Nature* **407**(6804), 608–610 (2000).
3. G. Jacobsen and P. Wildhagen, "A general and rigorous WDM receiver model targeting 10–40-gb/s channel bit rates," *J. Lightwave Technol.* **19**(7), 966–976 (2001).
4. J.-P. Laude, "DWDM fundamentals, components, and applications," pp. 19–82, Artech House, Boston, Massachusetts (2002).
5. B. S. Song, S. Noda, and T. Asano, "Photonic devices based on in-plane hetero photonic crystals," *Science* **300**(5625), 1537–1537 (2003).
6. B. G. Lee et al., "Characterization of a 4×4 gb/s parallel electronic bus to WDM optical link silicon photonic translator," *IEEE Photonics Technol. Lett.* **19**(7), 456–458 (2007).
7. S. H. Jeong, T. Yu, and K. Morito, "1 \times 4 channel SI-nanowire microring-assisted multiple delayline-based optical mux/demux," *J. Lightwave Technol.* **33**(17), 3736–3743 (2015).
8. S. Cheung et al., "Ultra-compact silicon photonic 512×512 25 GHz arrayed waveguide grating router," *IEEE J. Sel. Top. Quantum Electron.* **20**(4), 310–316 (2014).
9. Q. Fang et al., "WDM multi-channel silicon photonic receiver with 320 Gbps data transmission capability," *Opt. Express* **18**(5), 5106–5113 (2010).
10. S. Pathak, T. D. Van, and W. Bogaerts, "Design trade-offs for silicon-on-insulator-based AWGs for (de)multiplexer applications," *Opt. Lett.* **38**(16), 2961–2964 (2013).
11. J. Xiao, X. Liu, and X. Sun, "Design of an ultracompact MMI wavelength demultiplexer in slot waveguide structures," *Opt. Express* **15**(13), 8300–8308 (2007).
12. M. S. Rouified et al., "Ultra-compact mmi-based beam splitter demultiplexer for the NIR/MIR wavelengths of 1.55 μm and 2 μm ," *Opt. Express* **25**(10), 10893–10900 (2017).
13. Q. Zhu and B. Li, "Photonic crystal waveguide-based Mach-Zehnder demultiplexer," *Appl. Opt.* **45**(35), 8870–8873 (2006).
14. H. Ito et al., "Hitless tunable WDM transmitter using SI photonic crystal optical modulators," *Opt. Express* **23**(17), 21629–21636 (2015).
15. S. Wang et al., "Monolithically integrated reconfigurable add-drop multiplexer for mode-division-multiplexing systems," *Opt. Lett.* **41**(22), 5298–5301 (2016).
16. A. Y. Piggott et al., "Inverse design and demonstration of a compact and broadband on-chip wavelength demultiplexer," *Nat. Photonics* **9**(6), 374–377 (2015).
17. J. M. Yarrisonrice and M. Y. Tekeste, "High efficiency photonic crystal based wavelength demultiplexer," *Opt. Express* **14**(17), 7931–7942 (2006).
18. B. S. Song et al., "Resonant-wavelength control of nanocavities by nanometer-scaled adjustment of two-dimensional photonic crystal slab structures," *IEEE Photonics Technol. Lett.* **20**(7), 532–534 (2008).
19. B. Chen et al., "Compact 1×4 wavelength demultiplexer based on directional coupling of periodic dielectric waveguides," *Appl. Opt.* **51**(17), 3950–3956 (2012).
20. T. N. Nguyen et al., "100-gb/s wavelength division demultiplexing using a photonic crystal four-channel drop filter," *IEEE Photonics Technol. Lett.* **25**(9), 813–816 (2013).
21. Y. Takahashi et al., "Ultra-compact 32-channel drop filter with 100 GHz spacing," *Opt. Express* **22**(4), 4692–4698 (2014).
22. F. Meng et al., "Waveguide-integrated photonic crystal spectrometer with camera readout," *Appl. Phys. Lett.* **105**(5), 051103–051105 (2014).
23. Y. Zhuang et al., "Design of a DWDM multi/demultiplexer based on 2-D photonic crystals," *IEEE Photonics Technol. Lett.* **28**(15), 1669–1672 (2016).
24. Y. Ooka et al., "Ultrasmall in-plane photonic crystal demultiplexers fabricated with photolithography," *Opt. Express* **25**(2), 1521–1528 (2017).
25. J. S. Foresi et al., "Photonic-bandgap microcavities in optical waveguides," *Nature* **390**(6656), 143–145 (1997).
26. J. T. Robinson et al., "Ultrasmall mode volumes in dielectric optical microcavities," *Phys. Rev. Lett.* **95**(14), 143901 (2005).
27. P. Velha et al., "Ultra-high q/v Fabry-Perot microcavity on SOI substrate," *Opt. Express* **15**(24), 16090–16096 (2007).

28. P. B. Deotare et al., "High quality factor photonic crystal nanobeam cavities," *Appl. Phys. Lett.* **94**(12), 121106 (2009).
29. E. Kuramochi et al., "Ultrahigh-q one-dimensional photonic crystal nanocavities with modulated mode-gap barriers on SiO₂ claddings and on air claddings," *Opt. Express* **18**(15), 15859–15869 (2010).
30. Q. Quan, P. B. Deotare, and M. Loncar, "Photonic crystal nanobeam cavity strongly coupled to the feeding waveguide," *Appl. Phys. Lett.* **96**(20), 203102 (2010).
31. J. D. Ryckman and S. M. Weiss, "Low mode volume slotted photonic crystal single nanobeam cavity," *Appl. Phys. Lett.* **101**(7), 071104 (2012).
32. M. J. Burek et al., "High quality-factor optical nanocavities in bulk single-crystal diamond," *Nat. Commun.* **5**, 5718 (2014).
33. R. Miura et al., "Ultralow mode-volume photonic crystal nanobeam cavities for high-efficiency coupling to individual carbon nanotube emitters," *Nat. Commun.* **5**, 5580 (2014).
34. D. Yang et al., "High sensitivity and high q-factor nanoslotted parallel quadrabeam photonic crystal cavity for real-time and label-free sensing," *Appl. Phys. Lett.* **105**(6), 063118 (2014).
35. D. Yang, C. Wang, and Y. Ji, "Silicon on-chip one-dimensional photonic crystal nanobeam bandgap filter integrated with nanobeam cavity for accurate refractive index sensing," *IEEE Photonics J.* **8**(2), 4500608 (2016).
36. D. Yang, C. Wang, and Y. Ji, "Silicon on-chip 1-D photonic crystal nanobeam bandstop filters for the parallel multiplexing of ultra-compact integrated sensor array," *Opt. Express* **24**(15), 16267–16279 (2016).
37. D. L. Kwong et al., "Cascade wide-angle y-junction 1 × 16 optical power splitter based on silicon wire waveguides on silicon-on-insulator," *Opt. Express* **16**(26), 21456–21461 (2008).
38. L. L. Wang et al., "Design and fabrication of a low-loss and asymmetric 1 × 5 arbitrary optical power splitter," *Appl. Opt.* **55**(30), 8601–8605 (2016).
39. J. D. Joannopoulos et al., *Photonic Crystals: Molding the Flow of Light*, Princeton University Press, Princeton (2008).
40. T. Pan et al., "Analysis of an electro-optic modulator based on a graphene-silicon hybrid 1-D photonic crystal nanobeam cavity," *Opt. Express* **23**(18), 23357–23364 (2015).
41. A. Hosseini et al., "Optimum access waveguide width for 1 × n multi-mode interference couplers on silicon nanomembrane," *Opt. Lett.* **35**(17), 2864–2866 (2010).

Daquan Yang is an associate professor at the University of Posts and Telecommunications (BUPT). He received his BS degrees in electronic information science and technology from the University of Jinan in 2005, and his PhD in optics from BUPT in 2014. He is the author of more than 50 journal and conference papers. His current research interests include photonics crystal, optical microcavity sensors, and photonic integrated devices.

Xin Chen is a postgraduate student at the University of Posts and Telecommunications (BUPT). He received his BS degree in electronic information engineering from the Wuhan University in 2015. His current research interest is focused on nanofiber-based photonic crystal integrated devices and systems.

Xuan Zhang works at the School of Information and Communication Engineering at the University of Posts and Telecommunications (BUPT). She received her bachelor's degree from Shandong University in 2008 and master's degree from BUPT in 2011. Her current research focuses on photonic crystal sensors and devices.